Stemming zone fragmentation analysis of optimized blasting with top-column air decks

E. Kabwe
School of Civil, Environmental & Mining Engineering, University of Adelaide, Adelaide, Australia

W. Banda
School of Mines, University of Zambia, Lusaka, Zambia

https://doi.org/10.15834/2018.1

ABSTRACT Trial application of air decks on a production shot improved fragmentation (32% reduction in x_{50}). Empirical fragmentation models and digital image processing software were used to estimate fragment size distribution of the blasted muck pile. The x_{20}, x_{50}, and x_{80} passing fractions, and top size were 42, 265, 683, and 1,455 mm, respectively. Air-deck application reduced explosives load in blastholes, lowering total charging cost by US$20/hole (15% decrease) and the powder factor to an average of 0.86 kg/m^3 (12% decrease). Blast results were 443,624 t of blasted material from the block (90% of total muck pile) was smaller than 900 mm.

■ **KEYWORDS** Air deck, Blasting, Fragmentation models, Gasbag, Stemming zone, Uniformity factor

RÉSUMÉ L'application pilote de trous d'air dans le cadre du coup de mine effectué pour commencer la production a amélioré la fragmentation (une réduction de 32 % des x_{50}). Des modèles empiriques de fragmentation et un logiciel de traitement numérique des images ont permis d'estimer la composition granulométrique des fragments du tas de déblais abattus. Les fractions de passé de crible de x_{20}, x_{50}, x_{80} et la dimension supérieure étaient représentées par des dimensions respectives de 42, 265, 683 et 1 455 mm. L'application de trous d'air a permis de diminuer la charge d'explosifs nécessaires dans les trous de mine, réduisant ainsi les coûts totaux de chargement de 20 $ US/trou (soit une réduction de 15 %) ainsi que le facteur de chargement (facteur poudre) à une moyenne de 0,86 kg/m^3 (soit une réduction de 12 %). Les coups de mine ont résulté en 443 624 tonnes de matériaux abattus du bloc (soit 90 % du tas de remblais total) mesurant moins de 900 mm.

■ **MOTS CLÉS** abattage à l'explosif, ballon à gaz, facteur d'uniformité, modèles de fragmentation, trou d'air, zone de bourrage

INTRODUCTION

The main objectives of production blasting are to achieve optimum rock fragmentation and to minimize overall production costs. Because blast fragmentation significantly affects the profitability of a mine, blasting is the first step of the size reduction in mining: An optimum size distribution is required to maximize the performance of mining and subsequent milling processes. If the fragmentation size distribution can be modelled and controlled, operations performance will improve. Blast fragmentation modelling is important in mine-to-mill optimization: It allows the estimation of blast fragmentation distributions that can be modelled in downstream mining processes to determine the optimum blast design.

Ideal rock fragmentation in blasting operations reduces the workload and improves the energy efficiency of milling (Hall & Brunton, 2002; Kanchibotla, 2003; Siddiqui, Ali Shah, & Behan, 2009). In blasting, explosives deliver an extreme source of energy that usually exceeds the level required to cause adequate breakage in the adjacent rock mass. Charge configurations play a substantial role in attaining the required blasting performance. In charge blasting, as a full column of explosive detonates, the initial pressure that arises in the explosive products greatly exceeds the strength of the rock mass. The resulting stress wave propagates into the rock medium, breaking it into very small particles (Jhanwar, 2011, 2012). Because of this intense and excessive crushing of the rock, a large portion of the explosive energy is wasted in an area near the charge (Chiappetta & Mammele, 1987).

To maintain desirable fragment sizes, air-deck blasting has been tested and applied. Air decking is a technique that creates an air gap in a blasthole. Air gaps can be positioned at the bottom (bottom-column), middle (mid-column), or top (top-column) of the charge column. Initially, air decks were used in surface blasting as a means of distributing the explosives energy more evenly throughout the rock mass that was being blasted (Sazid & Singh, 2013). Today, the application of air decks is being used successfully to allow reductions from 10 to 30% of the total explosives required for production blasting. Other applications of air decking include wall control and presplitting. In all these cases, air decking can result in significant savings and improved efficiencies over conventional methods (Sharma, 2010). In this study, a blasting trial was conducted by using a top-column air deck coupled with gasbags to investigate its influence on stemming zone fragmentation and reductions in the quantities and costs of stemming material, powder factor, and other blasting variables. Further, a fragmentation analysis was carried out using proposed empirical fragmentation models and Split-Desktop® (Split Engineering, 2001), a digital image processing software package.

Theory of air decking

When an explosive charge in a blasthole is detonated, the blasthole expands due to high pressure, crushing the borehole walls. A stress wave with high peak pressure propagates outward in all directions in the form of a compressive stress wave. According to Melnikov and Marchenko (1971), an air deck between sections of an explosive column results in an excitation of secondary waves that diffuse into the previously compressed rock. The charge structure ensures multiple impacts of stress waves into the ambient medium and, at the same time, changes the nature of energy transfer to the strained rock mass, which leads to an increase of the effective explosion energy in the medium. Once an air deck is positioned in the explosive column, it was also established that the peak borehole pressure decreases due to wave collision in the air gap. This might result in more energy transferred to the medium compared to blasting a continuous charge; hence, improved rock fragmentation can be achieved by employing an air gap in the explosive column of a blasthole. Marchenko (1982) concluded that the application of air decks substantially reduced the stresses in the air-deck zone as well as the crushing zone around the explosive charge, improving the degree of fragmentation. According to Moxon et al. (1993), no significant effect on the degree of fragmentation was observed with the air decks, which occupied 40% or less of the maximum volume of explosive. Jhanwar and Jethwa (2000) determined that air-deck blasting results in better fragmentation and improved use of explosive energy. Jhanwar et al. (2000) determined that the degree of fragmentation resulting from air-deck blasting is better than that of conventional blasting. Air-deck blasting was also established to be more effective in very low to low-strength, moderately jointed rocks compared to medium-strength, highly jointed rocks. Blastholes with air decks consumed less explosives than those with a conventional charge.

The types of air decks normally used are bottom-column, mid-column, and top-column. Figure 1a shows the top-column air deck design using a gasbag as a stemming enhancer. Jhanwar and Jethwa (2000) alleged that a bottom-column air deck can only be used to blast holes in soft and medium-strength rocks, concluding that when an air deck is employed at the top of the explosive column, it generates an improved degree of rock fragmentation in the stemming zone. Jhanwar (2011) proposed that air decks work best if positioned in the middle of an explosive column for general application, and at the top column for adequate breakage in the collar zone. He also pointed out that an air deck induces a change in the mechanism of explosive energy transfer to the rock mass. The energy transfer takes place in a series of pulses, which increases the duration over which explosive energy acts over the rock mass. This shows that air-deck length is critical to fragmentation. Moxon et al. (1993) concluded that the middle position of the air deck improved the degree of rock fragmentation due to the interaction of two concurrent stress-wave fronts from the top and bottom of an explosive charge; however, Chiap-

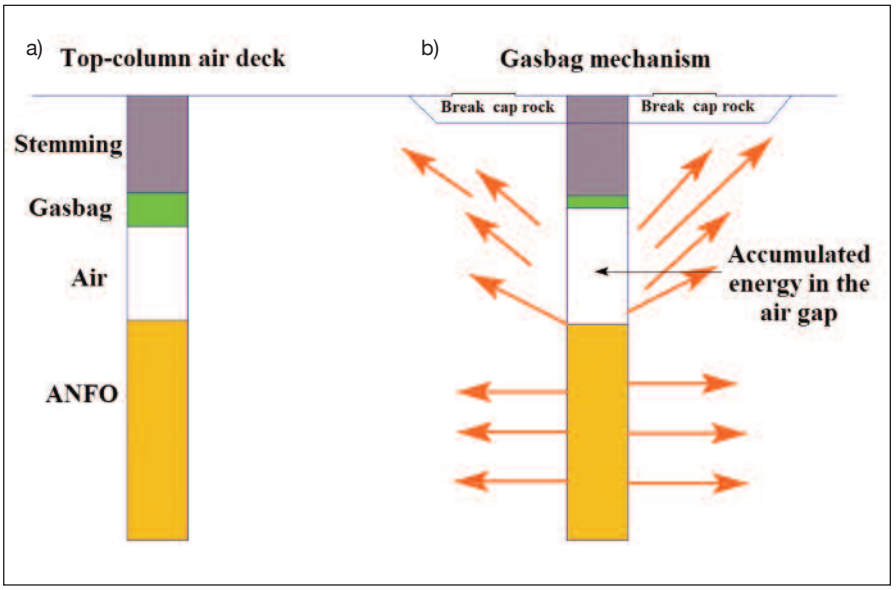

Figure 1. a) Schematic of a top-column air deck (ANFO: ammonium nitrate, fuel oil) and b) a gasbag mechanism used as a stemming enhancer, which releases energy in pulses (shown by orange arrows)

petta (2004) stated that the bottom-column air deck could be used more effectively because it produces more pressure at the bottom of the hole. After performing a series of numerical simulations to investigate the physical processes and effects in rock blasting with air-decked explosive charges, Liu and Katsabanis (1996) concluded the best blasting results were obtained with the longest air deck, provided the shortened stemming could confine the explosion gas in the blasthole.

Air-gap and gasbag employment reduces the amount of explosives per hole, thus decreasing explosive costs up to 30%. Top-column air decks are the most suitable where improved stemming region fragmentation is required. Gasbags serve as stemming enhancers, where they lock and prevent energy and gasses from escaping, and they then release the energy in separate pulses (Figure 1b).

Fragmentation models

A number of researchers proposed empirical models to estimate fragmentation size distribution. The models use equations to calculate the average fragment size (x_{50}) and fragment size distribution curves. They use input parameters such as the weight strength of explosives, geometric blast design features, and rock properties. Explosive properties and blast geometry features are easy to obtain and can be accurate; however, rock properties are difficult to establish—in most cases, assumptions must be made. This reduces the model's ability to accurately produce the fragment size distribution curve (Demenegas, 2008). In this study, three models will be used to determine the fragmentation distribution and results will be compared. A brief description of each model is given in this section.

In 1973, Larsson proposed equation 1 to predict the mean particle size of fragmentation (cited in Bakhtavar et al., 2015):

$$x_{50} = s' \times e^{\left(0.58 \times lnB - 0.145 \times ln(S/B) - 1.18 \times ln(q/c)^{-0.82}\right)} \quad (1)$$

where x_{50} is the mean particle size (in cm), s' is the blastability constant, B is the burden (in m), S is the spacing (in m), q is the specific charge (in kg/m^3), and c is the rock constant.

Hjelmberg (1983) proposed the SveDeFo model as an upgrade of Larsson's model. Additional to the parameters in equation 1, bench height and stemming length were considered for the mean fragment size prediction:

$$x_{50} = s' \left[1 + 4.67(T/L)^{2.5}\right] e^{\left(0.29 \times lnB^2(\sqrt{S}/1.25) - 1.18 \times ln(q/c)^{-0.82}\right)} \quad (2)$$

where T is the stemming length (in m) and L is the hole length (in m).

Cunningham (1983) proposed a simple and effective model for estimating fragmentation results, based on the expressions constructed by Kuznetsov (1973) and Rosin and Rammler (1933). It provides a method for calculating the mean fragment size and rock uniformity. Kuznetsov (1973) suggested the following empirical equation to predict the mean fragmentation size resulting from rock blasting:

$$x_m = AK^{-0.8}Q^{\frac{1}{6}}\left[\frac{115}{RWS}\right]^{\frac{19}{30}} \quad (3)$$

where x_m is the mean fragment size (in cm), A is the rock factor (between 0.8 and 22, depending on rock hardness and structure; its derivation is given in equation 4), K is the powder factor (in kg/m^3), Q is the mass explosive in the hole (in kg), and RWS is the explosive weight strength relative to ammonium nitrate, fuel oil (ANFO; in %). The relation between the rock factor (A) and blastability index (BI) proposed by Lilly (1986) can be obtained from equation 4, where BI is determined from equation 5:

$$A = 0.06 \times BI \quad (4)$$

$$BI = 0.5 \times (RMD + JPS + JPO + SGI + HD) \quad (5)$$

where RMD is the rock-mass description, JPS is the joint plane spacing, JPO is the joint plane orientation, SGI is the specific gravity influence (in t/m^3), and HD is the hardness factor. Inserting the blastability index, the model is presented as

$$x_m = 0.06 \times BI \times K^{(-0.8)}Q^{\left(\frac{1}{6}\right)}\left[\frac{115}{RWS}\right]^{\left(\frac{19}{30}\right)} \quad (6)$$

The Rosin-Rammler (Rosin & Rammler, 1933) equation is then used to predict the fragment size distribution resulting from rock blasting:

$$P(x_1) = exp\left[-0.693\left(\frac{x}{x_c}\right)^n\right] \quad (7)$$

where $P(x_1)$ is the proportion of the material larger than x, $x_m = (x_{50})$ is the characteristic size (in cm), and n is the uniformity index. The final equation of the Kuz-Ram model is an equation for the uniformity index:

$$n = \left(2.2 - 14\frac{B}{d}\right)\left(1 - \frac{SD}{B}\right)\sqrt{0.5\left(1 + \frac{S}{B}\right)}\left[\frac{|L_b - L_c|}{L_{tot}} + 0.1\right]^{0.1}\left(\frac{L_{tot}}{H}\right) \quad (8)$$

where B is the burden (in m), S is the spacing (in m), d is the borehole diameter (in mm), L_b is the bottom charge length (in m), L_c is the column charge length (in m), L_{tot} is the total charge length (in m), H is the bench height (in m), and SD is the standard deviation of drilling precision (in m). The SD value is determined from equation 9 and drilling accuracy:

$$SD = \frac{100 - \text{drilling accuracy}}{100} \times S \quad (9)$$

The n value determines the shape of the Rosin-Rammler curve and varies between 0.8 and 1.5. A high value indicates uniform sizing whereas a lower value indicates a larger proportion of fine and coarse material (Gheibie, Aghababaei, Hoseinie, & Pourrahimian, 2009). Experience has shown that this model predicts the coarse end reasonably well, but it can significantly underestimate the amount of fines generated (Ouchterlony, 2005). Spathis (2004) observed that the uniformity indices in the Kuz-Ram model were between 0.8 and 2.2, and the characteristic sizes of the model were in error between 105% and 179%. This led to model extensions, which involved one Rosin-Rammler function for the coarse material and another to improve the prediction of fines. The Julius Kruttschnitt Mineral Research Centre (JKMRC) proposed two empirical models to improve on the Kuz-Ram model's inability to predict the fragment size distribution: the crush zone model (CZM; Kanchibotla, Valery, & Morrell, 1999) and the two-component model (TCM; Djordjevic, 1999). In a later paper about the Kuz-Ram model, Cunningham (2005) made several changes to the prediction equation and pointed out the inability of the model to estimate fines, concluding that the only way to obviate the limitation was by adopting the model extensions.

Kanchibotla et al. (1999) proposed the CZM model, which applies two Rosin-Rammler functions to estimate the fragment size distribution curve: one to predict the fines part of the curve and the other to describe the coarse part of the curve (Gheibie et al., 2009). The two curves join at a fragment size (x_c), depending on the rock properties. The coarse part of the curve is represented by

$$P(x) = 1 - e^{\left(ln(1-P(x_c))\left(x/x_c\right)^{n_{coarse}}\right)} \quad (10)$$

where $P(x)$ is the percentage of material passing sieve size x (in %), x is the sieve size (in m), $P(x_c)$ is the percentage of material passing characteristic size x_c (in %), x_c is the characteristic size (in m), and n_{coarse} is the uniformity index for the coarse part of the curve. The n_{coarse} value can be determined from

$$n_{coarse} = \left(2.2 - 14\left(\frac{B}{d}\right)\right)\sqrt{\left(\frac{\left(1+\frac{S}{B}\right)}{2}\right)\left(\frac{L_{tot}}{H}\right)} \quad (11)$$

where B is the burden (in m), S is the spacing (in m), d is the borehole diameter (in mm), L_{tot} is the total charge length (in m), and H is the bench height (in m).

The fine rock material lies in a cylindrical crushed zone around the blasthole in which particles are generated by being crushed due to compressive shear failure (Kanchibotla et al., 1999). The crushed zone radius is assumed to be the distance from the blasthole to the point where radial stresses exceed the compressive strength of the rock mass:

$$r_c = r\sqrt{\frac{P_d}{\sigma_c}} \quad (12)$$

where r_c is the crushed zone radius (in m), r is the blasthole radius (in m), σ_c is the compressive strength of the rock (in Pa), and P_d is the detonation pressure (in Pa). Detonation pressure is calculated by

$$P_d = \rho_c \frac{C_d^2}{4} \quad (13)$$

where P_d is the detonation pressure (in Pa), C_d is the velocity of detonation (in m/s), and p_c is the density of explosive material (in kg/m^3). The fraction of the crushed material is obtained from

$$F_c = \frac{M_o}{M} \quad (14)$$

where F_c is the fraction of rock mass that fails in tension, M_o is the mass of rock that fails in compression (in kg), and M is the total mass of rock per blasthole (in kg). The fine part of the size distribution curve is predicted by

$$P(x) = 1 - e^{\left(ln(1-P(x_c))\left(\frac{x}{x_c}\right)^{n_{fine}}\right)} \quad (15)$$

where $P(x)$ is the percentage of material passing sieve size x (in %), x is the sieve size (in m), $P(x_c)$ is the percentage of material passing characteristic size x_c (in %), x_c is the characteristic size (in m), and n_{fine} is the uniformity index for the fine part of the curve. The n_{fine} value can be determined from

$$n_{fine} = \frac{ln\left(\frac{ln(1-F_c)}{ln\left(1-P(x_c)\right)}\right)}{ln\left(\frac{1}{x_c}\right)} \quad (16)$$

where F_c is the fraction of crushed material, $P(x_c)$ is the percentage of material passing characteristic size x_c (in %), x_c is the characteristic size (in mm), and n_{fine} is the uniformity index for the fine part of the curve.

The TCM model proposed by Djordjevic (1999) applies the two Rosin-Rammler functions simultaneously to predict the fine and coarse components of the size distribution curve. It is a five-parameter model in which two of the

parameters represent the coarse fraction, one represents the fines fraction, and the remaining two are related to the fines part of the distribution curve. The fragmentation curve in the TCM models is given by equation 17:

$$P(x) = 100\left(1-(1-F_c)e^{-ln2\left(\frac{x}{a}\right)^b}-F_c e^{-ln2\left(\frac{x}{c}\right)^d}\right) \quad (17)$$

where $P(x)$ is the percentage of material below size x, x is the size of material (in m), F_c is the fraction of crushed material, a is the mean fragment size outside the crushed zone (in m), b is the uniformity coefficient outside the crushed zone, c is the mean fragment size within the crushed zone (in m), and d is the uniformity coefficient within the crushed zone. Parameters a and b are similar to the Kuz-Ram model parameters x_{50} and n; the fraction of the crushed material is determined the same way as in the CZM. The crushed zone radius in the TCM model is predicted by

$$r_c = \left(\frac{r}{\sqrt{\frac{24TS_{insitu}}{P_b}}}\right) - r \quad (18)$$

where r_c is the crushed zone radius (in m), r is the blasthole radius (in m), P_b is the detonation pressure (in Pa), and TS_{insitu} is the in-situ tensile strength (in Pa). The pressure of detonation is determined the same way as in the CZM model, with the in-situ tensile strength determined by

$$TS_{insitu} = \sigma_\tau\left(\frac{0.05}{mean\ block\ size}\right)^{0.18} \quad (19)$$

where σ_τ is the tensile strength of rock (in MPa) and the mean block size is in m.

Ouchterlony (2005) proposed the Kuznetsov-Cunningham-Ouchterlony (KCO) model to predict the fragment size distribution by replacing the original Rosin-Rammler equation with the Swebrec© function (equation 20). The fines part of the fragment size distribution received a more satisfactory prediction when the Swebrec function was introduced (Ouchterlony, 2016). Like the Rosin-Rammler model, the KCO model uses the 50% passing value (x_{50}) as the central parameter, while also introducing an upper limit to fragment size x_{max} and b, a curve undulating parameter similar to n in the Kuz-Ram model (Gheibie et al., 2009). The equation for x_{50} remains the same; the equation for b and the Swebrec function is given by

$$P(x) = \frac{1}{\left(1+\left[\frac{ln\left(\frac{x_{max}}{x}\right)}{ln\left(\frac{x_{max}}{x_{50}}\right)}\right]^b\right)} \quad (20)$$

$$b = \left[2ln2 \times ln\left(\frac{x_{max}}{x_{50}}\right)\right]n \quad (21)$$

where $P(x)$ is the percentage of material passing sieve size x (in %), x is the sieve size (in cm), x_{50} is the 50% passing size (in cm), x_{max} is the maximum in-situ block size (in cm), and n is the uniformity index. Spathis (2004) rightly commented that Cunningham (1987) had misinterpreted the Kuznetsov (1973) formula for the mean fragment size, using it as a mean but later treating it as a median. Spathis (2004) suggested the addition of a prefactor to the Rosin-Rammler equation, proposing that x_{50} be

$$x_{50} / x = (ln2)^{1/n} / \Gamma\ (1+1/n) \quad (22)$$

where x_{50} is the 50% passing size (in cm), x is the sieve size (in cm), Γ is the gamma function, and n is the uniformity index.

Equation 23 represents the KCO model as an improved extension of the Kuz-Ram model to overcome the failure of predicting the fine range and the upper limit of particle size:

$$x_{50} = \left(\frac{(ln2)^{\frac{1}{n}}}{\Gamma\left(1+\frac{1}{n}\right)}\right) AK^{-0.8}Q^{\frac{1}{6}}\left[\frac{115}{RWS}\right]^{\frac{19}{30}} \quad (23)$$

Digital image processing

Digital image processing is used to measure blast fragmentation through digital images. Several digital image processing software packages—namely Split-Desktop, WipFrag™, FragScan, Technical University of Clausthal image processing system (TUCIPS), PowerSieve™, IPACS, and Waterloo image enhancement program (WIEP)—are commercially available to analyze the fragment size distribution (Ozkahraman, 2006). The image processing software Split-Desktop (Split Engineering, 2001) was used for this study. Split-Desktop was designed to calculate the size distribution of rock fragments by analyzing greyscale images taken by a digital camera (Siddiqui et al., 2009). Image processing has several advantages: It can be completely automated, eliminating several process-related expenses; a great number of measurements can be made, increasing the overall reliability; and it can be used on a continuous basis without affecting the production cycle (Sanchidrián, Segarra, Ouchterlony, & López, 2009). Some errors, however, are associated with image processing software, due mainly to these reasons:

- Image analysis can only process what can be seen with the naked eye and does not take into account the internal composition of a blasted muck pile, thus sampling strategies should be carefully considered.
- Analyzed particle size can be overdivided or overcombined: larger particles can be divided into smaller parti-

cles, and smaller particles can be combined into larger particles. In this case, manual editing is required.
- Very fine particles can be underestimated, especially from a muck pile after blasting.

Errors can be minimized by using established sampling methods, a proper sampling environment, and site-specific calibration of the image processing software (Maerz, 1999; Maerz & Zhou, 2000). The most reliable way for fragmentation to be assessed is through sieving the entire muck pile, which is nearly impossible.

TRIAL SITE

The blast was conducted at the Chimiwungo open pit, part of the Lumwana project located in the northwestern province of Zambia. Hosted within the Mwombezhi basement dome in the western arm of the Neoproterozoic Lufilian Arc thrust fold belt, it comprises the Chimiwungo main, south, and north mineralized zones (Stroud, 2010). The conventional blast practice revealed problems related to poor blast performance, which has been the major challenge at the pit. This includes poor fragmentation in the stemming zone, a tendency for uncontrolled fly rock, premature ejections, and an elevated cost of explosives and stemming material.

Table 1. Rock-mass properties determined using RocData® (Rocscience, 2013; GSI, geological strength index)

Dominant rock type	Gneiss
Hoek-Brown classification	
Intact uniaxial compressive strength (MPa)	189
GSI	55
m_i	28
Disturbance factor	0
Hoek-Brown criteria	
m_b	5.613
s	0.0067
a	0.504
Failure envelope range	
σ_3 max (MPa)	47.25
Unit weight (MN/m^3)	0.026
Mohr-Coulomb fit	
Cohesion (c; MPa)	13.7
Friction angle (φ;°)	40.94
Rock-mass parameters	
Tensile strength (MPa)	–0.227
Uniaxial compressive strength (MPa)	15.203
Global strength (MPa)	60.05
Modulus of deformation (MPa)	13,335
Poisson ratio (v)	0.235

Table 2. Rock-mass rating of the blast shot (Bieniawski, 1989)

General conditions	
Intact rock strength (MPa)	100–250
RQD (%)	75–90
Discontinuity spacing (m)	0.6–2.0
Discontinuity orientation	Favourable
Groundwater conditions	Wet
Discontinuity conditions	
Length (m)	< 1 m
Separation (mm)	< 0.1
Roughness	Slightly rough
Infill (mm)	Hard < 5
Weathering	Moderate
Rock-mass rating	70
Rock-mass classification	Class II—good rock

MATERIALS AND METHODS

A top-column air-deck blast trial was conducted simultaneously with a conventional blast. General ground conditions and a rock-mass rating of the trial area were determined (Tables 1 and 2). The blast design parameters on the conventional and the top-column air-deck blasts were kept similar. Table 3 shows the drilling accuracy results used to determine the SD value.

Blast design and parameters

The blast design was based on a 3.5 m stemming height and 0.92 kg/m^3 powder factor, but after introducing the top-column air deck, these were reduced to 2.5 m and 0.74 kg/m^3, respectively. The blast design parameters used are given in Table 4. Figures 2 and 3 illustrate the explosive

Table 3. Drilling precision results for standard deviation determination

Drill rig (DR)	**Drilling accuracy (%)**
DR05	90
DR06	79
DR07	82
DR08	82
DR10	83
DR11	78
DR12	100
Average	85
Average DR penetration rate (m/h)	22
% re-drills	15

Table 4. Blast design parameters and explosive properties (Abbreviations: ANFO, ammonium nitrate, fuel oil; RWS, Relative weight strength; VOD, velocity of detonation)

Blast design parameters	**Top-column air deck**	**Conventional**
Hole diameter (mm)	165	165
Bench height (m)	12	12
Subdrilling (m)	0.5	0.5
Burden (m)	4.2	4.2
Spacing (m)	4.5	4.5
Stemming (m)	2.5	3.5
Blasting pattern	Square	Square
Initiation system	Nonel or shock tube	Nonel or shock tube
Powder factor (kg/m^3)	0.72	0.92
Explosive properties		
Explosive	SD135 (emulsion)	SD135 (emulsion)
Explosive column length (m)	8.0	9.0
Density (g/cm^3)	1.25	1.25
VOD (m/s)	4,750	4,750
RWS (ANFO = 100)	80	80

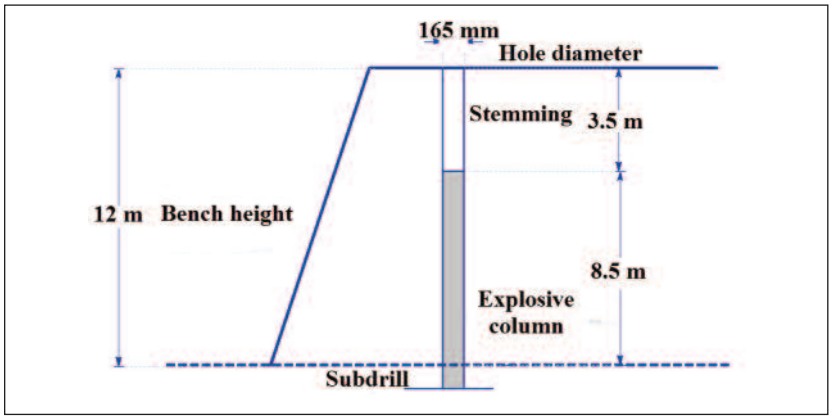

Figure 2. Explosive loading for a conventionally charged hole

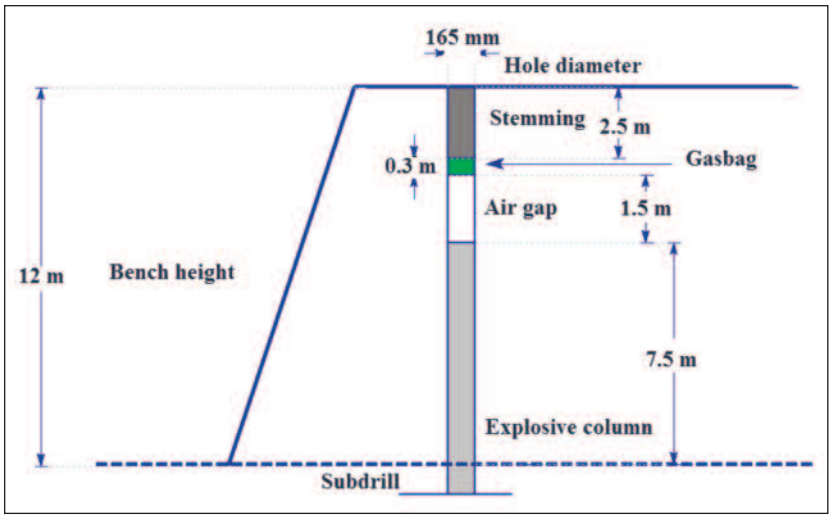

Figure 3. Explosive loading for a top-column air deck with gasbag-charged hole

loading for conventional and top-column air-deck blastholes, respectively.

The designed subdrill was 0.5 m, which was short relative to the burden. When the subdrill is short, the area of maximum tension in a blasthole during blasting will be located higher up and will not break to the bottom of the floor. The rule of thumb in conventional blasting is that subdrill depth (in m) should be the ratio of the burden (Nobel, 2010):

$$subdrill = 0.3 \times B \approx 1.3 \quad (24)$$

where B is burden thickness (in m).

Based on the burden's stiffness ratio, the size distribution of the muck pile can be estimated. The stiffness ratio is also a major factor when calculating the spacing for bench blasting applications. The burden stiffness ratio predicts the degree of fragmentation if all blast and bench parameters are to standard:

$$burden\ stiffness\ ratio = H/B \approx 2.9 \quad (25)$$

where H is the bench height (in m) and B is the burden (in m).

The ratio values of 2–3.5 and > 3.5 represent good and very good fragmentation, respectively (Nobel, 2010). The burden stiffness ratio value determined from equation 25 was 2.9; this predicted the degree of fragmentation for the rock to be blasted. The cost of charging the conventional charged hole was higher than a gasbag-charged hole. Table 5 shows that the introduction of the top-column air deck with gasbags reduced the quantity and cost of most blasting variables:

$$volume\ blasted\ per\ hole = B \times S \times H \approx 226.8 \quad (26)$$

where the volume blasted per hole is in m^3, B is the burden (in m), S is the spacing (in m), and H is the bench height (in m).

Table 6 shows that there were fewer holes drilled as compared to the number of holes marked out, but the volume of pumped emulsion was actually higher than planned, as a result of backfilling overdrilled holes with drill chippings instead of aggregate; the emulsion basically mixed with chippings and thus overcharged the holes.

Blasting

The top-column air deck blast was fired simultaneously with a conventional blast for assessment (Figure 4). It was observed that the conventional blast experienced premature ejections and the muck pile showing uneven fragmentation (Figure 5), as compared to the top-column air-deck blast.

Table 5. Cost of blasting per hole

	Conventional blasthole	Top-column air-deck blasthole
Explosives cost (US$)	187.75	165.75
Stemming cost ($)	2.28	1.82
Gasbag cost ($)	–	2.89
Total cost per hole ($)	190.03	170.46
Volume blasted per hole (m^3)	226.8	226.8
Powder factor (kg/m^3)	0.97	0.86

Table 6. Comparison of marked out and actual top-column air-deck blasting values

	Marked out	Actual
Number of holes blasted	756	722
Pumped emulsion (kg)	136,477	146,583
Powder factor (kg/m^3)	0.77	0.89
Blasted material (t)	473,063	443,624

The top-column air deck–blasted muck pile was evenly fragmented (Figure 6).

ANALYSES AND RESULTS

Fragmentation model analysis

Based on the crushers at the mine, the allowable size classification is shown in Table 7. In the Kuz-Ram model, the predicted average x_{50} size is 324 mm for the top-column air-deck blast and 348 mm for the conventional blast. The uniformity factor was 1.30 for the top-column air-deck blast and 1.073 for the conventional blast. The proportion of material larger than 900 mm, $P(x_{90})$, was approximately 7 and 11% for the top-column air-deck and conventional blasts, respectively (Table 8).

In the KCO model, the average fragment size is 303 mm and the curve undulating parameter is $b = 3.172$ for the top-column air-deck blast, whereas for the conventional blasted

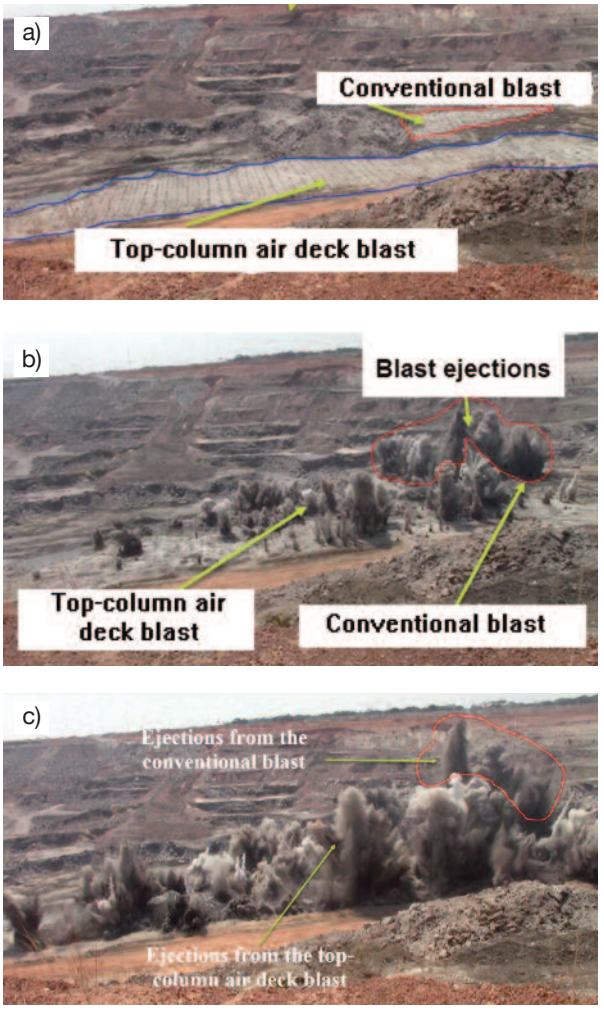

Figure 4. a) Location of the charged top-column air deck and conventional blasts, b) rock ejections after blast detonation, and c) rock ejections at a later time after blast detonation

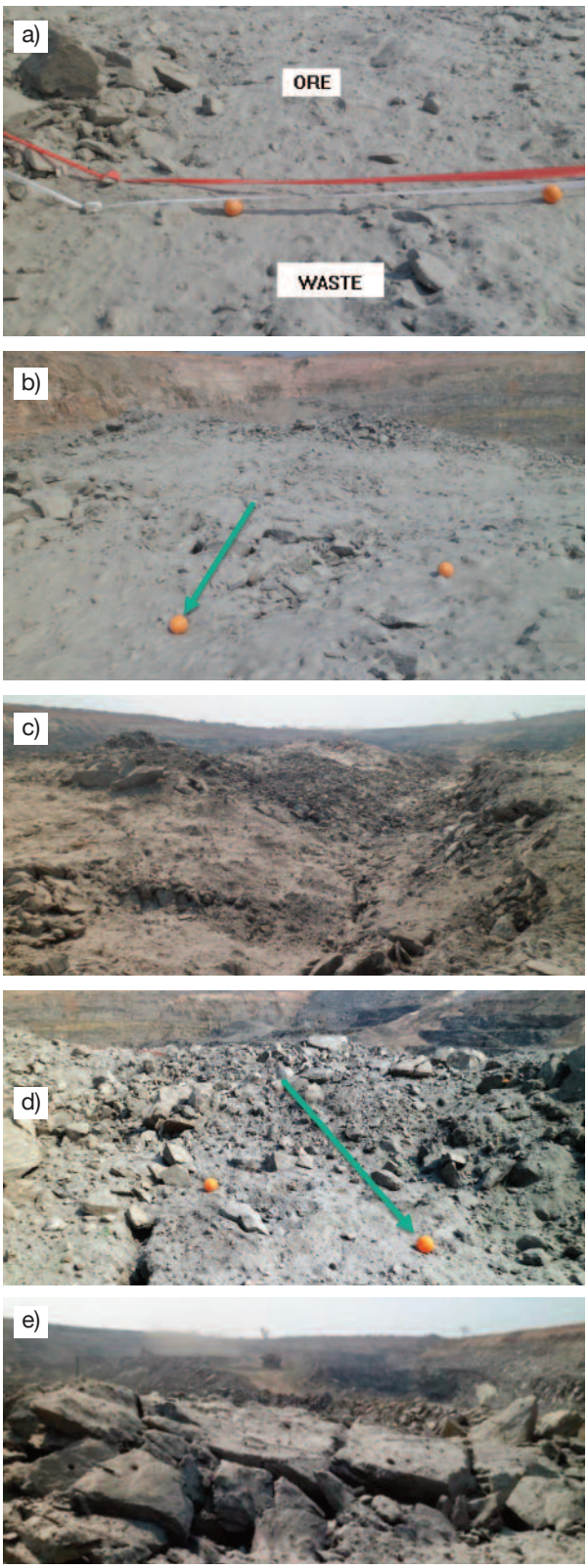

Figure 5. Conventional blasted muck pile, showing uneven fragmentation. In a), the red tape indicates the portion of the muck pile with ore and the white tape indicates the portion of the muck pile with waste. The green arrows in b) and d) point to the scaling ball used for fragmentation analysis.

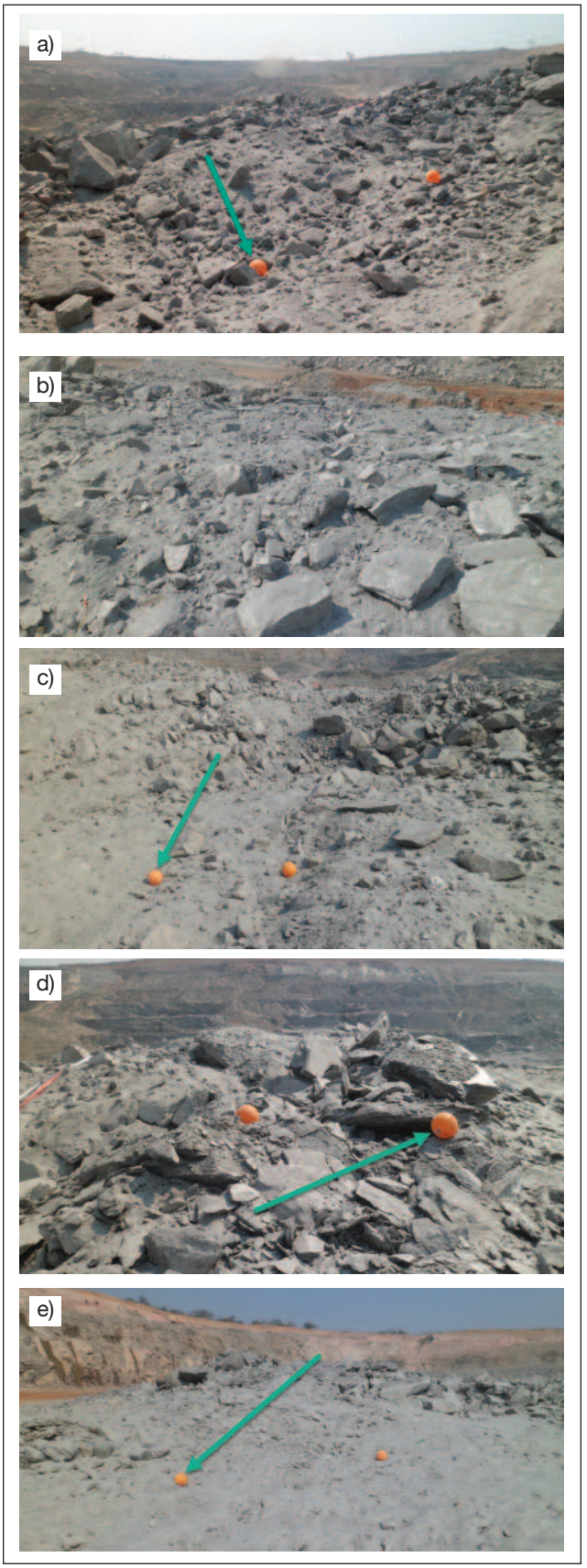

Figure 6. Top-column air deck–blasted muck pile, showing even fragmentation. The green arrows in a), c), d), and e) point to the scaling ball used for fragmentation analysis.

muck pile, the average fragment size is 282 mm and the curve undulating parameter is $b = 2.299$ (Table 9).

In the CZM model, the predicted average value of x_{50} is 27 mm for the top-column air-deck blast and 240 mm for the conventional blast. The uniformity factor for the fines part of the size distribution is 0.081 and 0.392 for the top-column air-deck blast and conventional blast, respectively, whereas the uniformity factor for the coarse part of the distribution is 1.973 and 1.329 for the top-column air-deck blast and the conventional blast, respectively (Table 10).

Digital image analysis

Twenty photographs were taken on both muck piles before mucking, after mucking, and every time a truck was loaded. The images were analyzed and processed with Split-Desktop (Split Engineering, 2001), to estimate size distribution results. Delineated images, size distribution results, and fragment size distribution curves are shown in Figures 7–9 and Tables 11 and 12.

The prediction values of the mean fragmentation from the empirical models are in range with those obtained from Split-Desktop image analysis (Tables 13, 14; Figures 10, 11). Split-Desktop results for conventional and air-deck

Table 7. Crusher material classification

Particle size (mm)	Classification
< 50	Overblasted material
50–800	Very fine material
800–1,100	Good crusher feed

Table 8. Kuz-Ram fragmentation model results

Parameter	Top-column air deck	Conventional blast
x_{50} (mm)	324	348
$P(x_{90})$ (%)	0.07	0.11
n	1.3	1.1
SD (m)	0.68	0.68

Table 9. Kuznetsov-Cunningham-Ouchterlony (KCO) fragmentation model results

Parameter	Top-column air deck	Conventional blast
x_{50} (mm)	303	282
b	3.172	2.299
n	2.03	1.573
Maximum fragment size	990	999

Table 10. Crush zone (CZM) fragmentation model results

Parameter	Top-column air deck	Conventional blast
x_{50} (mm)	27	240
n_{coarse}	1.973	1.329
n_{fines}	0.081	0.392

blasts were plotted on a graph, clarifying that air-deck fragmentation is as good as, or better than, conventional blast fragmentation (Figure 12).

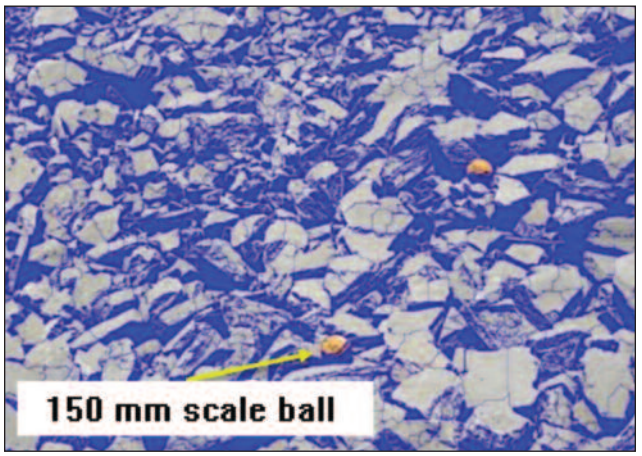

Figure 7. Digitization and delineation of sample photograph of the muck piles using Split-Desktop

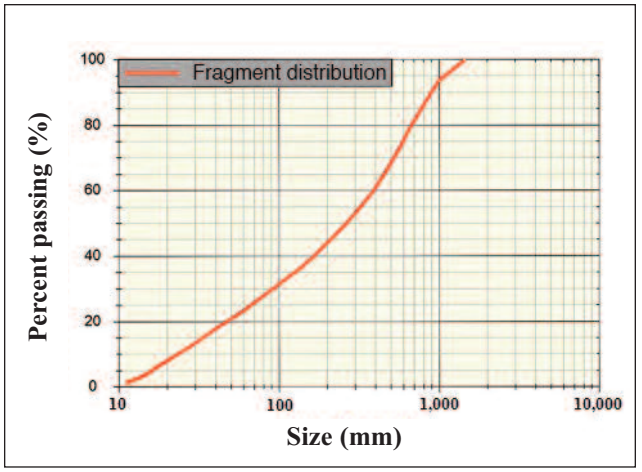

Figure 8. Top-column air-deck blast fragment size distribution curve from 10 analyzed photos of the muck pile

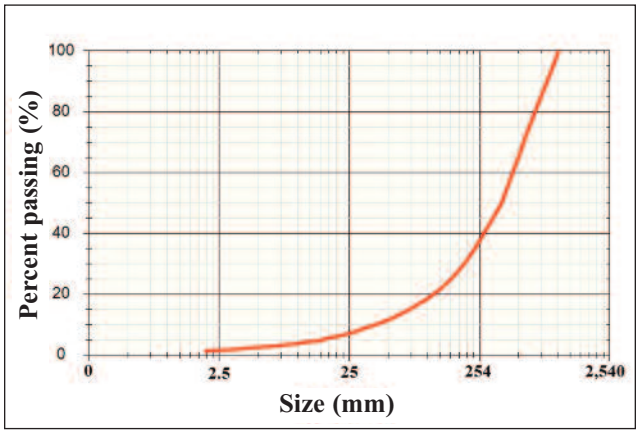

Figure 9. Conventional blast fragment size distribution curve from 10 analyzed photos of the muck pile

Table 11. Top-column air-deck blast cumulative size distribution results obtained from Split-Desktop

Size (mm)	% passing	% passing	Size (mm)
2,000	100	x_{10}	11
1,000	93	x_{20}	42
750	84	x_{30}	94
500	68	x_{40}	168
375	59	x_{50}	265
250	49	x_{60}	389
187	42	x_{70}	523
78.7	28	x_{80}	683
		x_{90}	899
		Top size (99.95%)	1,455

Table 12. Conventional blast cumulative size distribution results obtained from Split-Desktop

Size (mm)	% passing	% passing	Size (mm)
1,270	100	x_{10}	41
735	77	x_{20}	112
381	50	x_{30}	199
254	37	x_{40}	283
203	31	x_{50}	385
152	25	x_{60}	479
102	19	x_{70}	567
51	12	x_{80}	771
25	7.2	x_{90}	961
19	6	Top size (99.95%)	1,436

Table 13. Top-column air-deck blast fragment sizes according to different fragmentation models

Fragmentation model	x_{20} (mm)	x_{50} (mm)	x_{80} (mm)	Top size (mm)
Kuz-Ram	102	324	467	1,523
Kuznetsov-Cunningham-Ouchterlony	110	303	570	990
Crush zone	8.5	27	405	460
Split-Desktop	42	265	683	1,455

Table 14. Conventional blast fragment sizes according to different fragmentation models

Fragmentation model	x_{20} (mm)	x_{50} (mm)	x_{80} (mm)	Top size (mm)
Kuz-Ram	86	348	542	2,098
Kuznetsov-Cunningham-Ouchterlony	170	282	660	999
Crush zone	38	240	500	600
Split-Desktop	112	385	771	1,436

RESULTS

A substantial reduction in explosive load in conventional holes to top-column air-deck holes was obtained: 221 kg per hole to 195 kg per hole. The powder factor was reduced from 0.92 to 0.72 kg/m^3, as was the cost of explosive per hole, from US$187.75 to $165.75. The stemming cost decreased from $2.28 to $1.82 per hole, and the overall cost per hole decreased from $190.03 to $170.46, a reduction of approximately $20 per hole. Thus, the total reduction on the 722 holes blasted by the

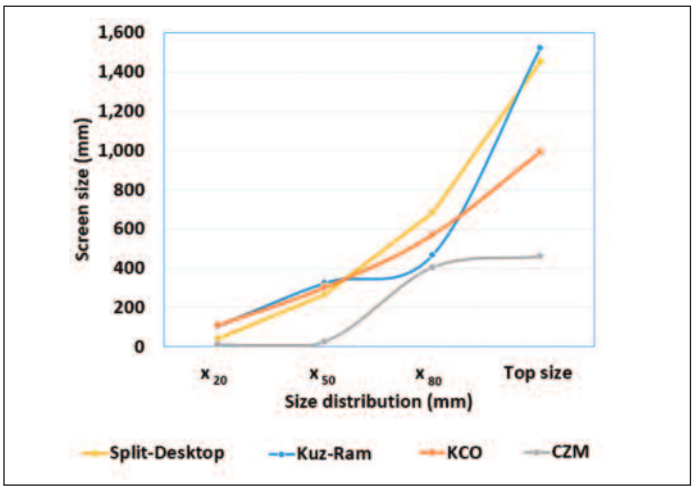

Figure 10. Comparison of fragmentation curves from top-column air-deck blast (CZM, crush zone model; KCO, Kuznetsov-Cunningham-Ouchterlony model)

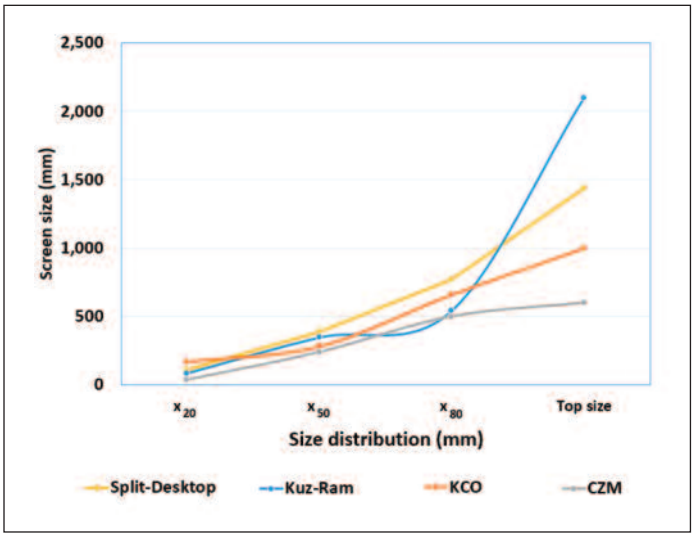

Figure 11. Comparison of fragmentation curves from conventional blast (CZM, crush zone model; KCO, Kuznetsov-Cunningham-Ouchterlony model)

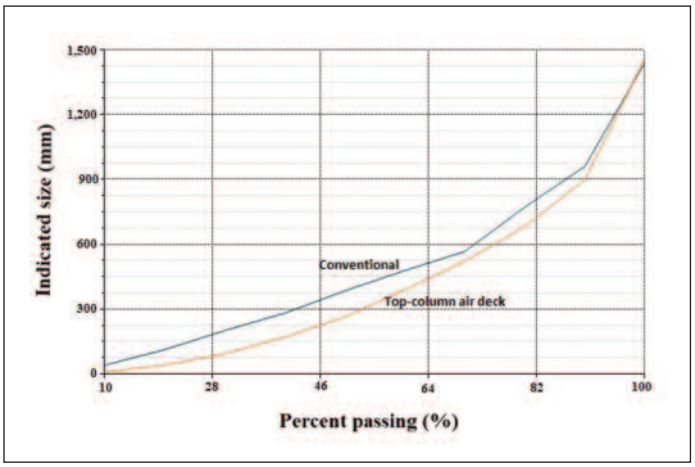

Figure 12 Comparison of Split-Desktop fragmentation results for conventional and air-deck blasts

application of a top-column air-deck was approximately $14,129.54, which accounts for an approximately 20% cost reduction, and which saved approximately $5.024/t blasted.

Results obtained from the analysis of muck-pile images using Split-Desktop showed that the mean fragment size was 265 mm, and x_{20}, x_{80}, and top size were 42, 683, and 1,455 mm, respectively. The optimum crusher feed size was 1,200 mm and a small fraction of the material was larger than 1,200 mm.

CONCLUSIONS

The blast conducted showed that on the top-column air deck–blasted muck pile, there was a substantial decrease in proportion of oversize fragment generation in the stemming area. The Rosin-Rammler uniformity index predicted value was 1.3; the obtained value confirmed uniform size distribution.

In the empirical fragmentation models, rock-mass input parameters are not easy to determine. Given the correct input parameters, fragmentation models do not consistently predict correct fragmentation because they capture some, but not all, of the important rock-mass and blast design parameters.

Values determined through the image analysis software for x_{20}, x_{50}, and x_{80} were close in range with predicted values from the empirical fragmentation models, which showed data consistency; however, an increase in sample space would allow for a better determination of the values.

The mine will benefit from the application of air decks in terms of cost savings, higher efficiency, and environmentally sound operations.

ACKNOWLEDGMENTS

The author thanks the volunteer peer reviewers for CIM, whose contributions improved the quality of this paper. Approval for publication by the Underground Mining Society of CIM is also appreciated. The author acknowledges the support of the Lumwana Mining Company, Zambia.

Paper reviewed and approved for publication by the Underground Mining Society of CIM.

Eugie Kabwe received his BSc (MinSc) in mining engineering from the University of Zambia, Lusaka, Zambia. He worked in the mining industry for more than five years and later earned his MEng in mining engineering from the University of Science and Technology Beijing, Beijing, China. He is currently a PhD student at the University of Adelaide, Adelaide, Australia. **eugie.kabwe@adelaide.edu.au**

Webby Banda is a Lecturer of Mineral Economics in the Department of Mining Engineering at the University of Zambia (UNZA). He holds a Bachelor of Mineral Sciences (BMinSc) degree and Master of Mineral Sciences (MMinSc) degree, both of which he obtained from UNZA.

REFERENCES

Bakhtavar, E., Khoshrou, H., & Badroddin, M. (2015). Using dimensional-regression analysis to predict the mean particle size of fragmentation by blasting at the Sungun copper mine. *Arabian Journal of Geosciences, 8*(4), 2111–2120. https://doi.org/10.1007/s12517-013-1261-2

Bieniawski, Z. T. (1989). *Engineering rock mass classifications: A complete manual for engineers and geologists in mining, civil, and petroleum engineering*. New York, NY: John Wiley & Sons.

Chiappetta, F. (2004). New blasting technique to eliminate subgrade drilling, improve fragmentation, reduce explosive consumption and lower ground vibrations. *Journal of Explosives Engineering, 21*(1), 10–12.

Chiappetta, R. F. & Mammele, M. E. (1987). Analytical high-speed photography to evaluate air decks, stemming retention and gas confinement in presplitting, reclamation and gross motion applications. *Proceedings of the Second International Symposium on Rock Fragmentation by Blasting*, Bethel, CT, 257–301.

Cunningham, C. V. B. (1983). The Kuz-Ram model for prediction of fragmentation from blasting. *Proceedings of the First International Symposium on Rock Fragmentation by Blasting*, Lulea, Sweden, Vol. 2, 439–453.

Cunningham, C. V. B. (2005). The Kuz-Ram fragmentation model—20 years on. In R. Holmberg et al. (Eds.), *Proceedings of the Brighton Conference*, Brighton, U.K., 201–210.

Demenegas, V. (2008). *Fragmentation analysis of optimized blasting rounds in the Aitik mine*, Master's thesis, Luleå University of Technology, Luleå, Sweden.

Djordjevic, N. (1999). A two-component model of blast fragmentation. *AusIMM Proceedings (Australia), 304*(2), 9–13.

Gheibie, S., Aghababaei, H., Hoseinie, S. H., & Pourrahimian, Y. (2009). Modified Kuz-Ram fragmentation model and its use at the Sungun copper mine. *International Journal of Rock Mechanics and Mining Sciences, 46*(6), 967–973. https://doi.org/10.1016/j.ijrmms.2009.05.003

Hall, J., & Brunton, I. (2002). Critical comparison of Julius Kruttschnitt Mineral Research Centre (JKMRC) blast fragmentation models. *Fragblast, International Journal for Blasting and Fragmentation, 6*(2), 207–220. https://doi.org/10.1076/frag.6.2.207.8670

Hjelmberg, H. (1983). Some ideas on how to improve calculations of the fragment size distribution in bench blasting. *Proceedings of the First International Symposium on Rock Fragmentation by Blasting*, Luleå, Sweden, 469–494.

Jhanwar, J. (2011). Theory and practice of air-deck blasting in mines and surface excavations: A review. *Geotechnical and Geological Engineering, 29*(5), 651–663. https://doi.org/10.1007/s10706-011-9425-x

Jhanwar, J. C. (2012). Investigation into the influence of air-decking on blast performance in opencast mines in India: A study. In A. K. Ghose & A. Joshi (Eds.), *Blasting in Mining—New Trends*. Boca Raton, FL: CRC Press, 105–110. https://doi.org/10.1201/b13739-14

Jhanwar, J. C. & Jethwa, J. L. (2000). The use of air decks in production blasting in an open pit coal mine. *Geotechnical and Geological Engineering, 18*(4), 269–287. https://doi.org/10.1023/A:1016634231801

Jhanwar J. C., Jethwa J. L., & Reddy A. H. (2000). Influence of air-deck blasting on fragmentation in jointed rocks in an open-pit manganese mine. *Engineering Geology, 57*(1–2), 13–29. https://doi.org/10.1016/S0013-7952(99)00125-8

Kanchibotla, S. S. (2003). Optimum blasting? Is it minimum cost per broken rock or maximum value per broken rock? *Fragblast, International Journal for Blasting and Fragmentation,* 7(1), 35–48. https://doi.org/10.1076/frag.7.1.35.14059

Kanchibotla, S. S., Valery, W., & Morrell, S. (1999). Modelling fines in blast fragmentation and its impact on crushing and grinding. *Explo '99—A conference on rock breaking,* Kalgoorlie, Australia, 137–144.

Kuznetsov, V. M. (1973). The mean diameter of the fragments formed by blasting rock. *Soviet Mining Science, 9*(2), 144–148. https://doi.org/10.1007/BF02506177

Lilly, P. A. (1986). An empirical method of assessing rock mass blastability. *Proceedings of Large Open Pit Planning Conference*, Parkville, Australia, 89–92.

Liu L., & Katsabanis P. D. (1996). Numerical modeling of the effects of airdecking/decoupling in production and controlled blasting. In B. Monhanty (Ed.), *Rock fragmentation by blasting*. Rotterdam, The Netherlands: Balkema, A. A., 319–330.

Maerz, N. H. (1999). Online fragmentation analysis: Achievements in the mining industry. *Proceedings of the Center for Aggregates Research (ICAR) Seventh Annual Symposium*, Austin, TX, C1-1-1–B1-1-10.

Maerz, N. H., & Zhou, W. (2000). Calibration of optical digital fragmentation measuring systems. *Fragblast, International Journal for Blasting and Fragmentation, 4*(2), 126–138. https://doi.org/10.1076/frag.4.2.126.7450

Marchenko, L. N. (1982). Raising the efficiency of a blast in rock crushing. *Soviet Mining Science, 18*(5), 395–399. https://doi.org/10.1007/bf02528444

Melnikov, N. V., & Marchenko, L. N. (1971). Effective methods of application of explosion energy in mining and construction. *Proceedings of the Twelfth US Symposium on Rock Mechanics,* 350–378.

Moxon, N. T., Mead, D., & Richardson, S. B. (1993). Air-decked blasting techniques: Some collaborative experiments. *Transactions of the Institution of Mining and Metallurgy*, *Section A*: *Mining Industry, 102*(1–3), A25–A30.

Nobel, D. (2010). *Blasting and explosives quick reference guide 2010*. Kalgoorlie, Australia: Dyno Nobel Asia Pacific Pty Limited. Retrieved from https://www.leg.state.mn.us/docs/2015/other/150681/PFEISref_1/Dyno%20Nobel%202010.pdf

Ouchterlony, F. (2005). The Swebrec© function: Linking fragmentation by blasting and crushing. *Transactions of the Institutions of Mining and Metallurgy, Section A: Mining Technology, 114*(1), 29–44. https://doi.org/10.1179/037178405X44539

Ouchterlony, F. (2016). The case for the median fragment size as a better fragment size descriptor than the mean. *Rock Mechanics and Rock Engineering, 49*(1), 143–164. https://doi.org/10.1007/s00603-015-0722-1

Ozkahraman, H. T. (2006). Fragmentation assessment and design of blast pattern at Goltas limestone quarry, Turkey. *International Journal of Rock Mechanics and Mining Sciences, 43*(4), 628–633. https://doi.org/10.1016/j.ijrmms.2005.09.004

Rocscience. (2013). RocData® [Computer software]. Toronto, ON: Author.

Rosin, P. & Rammler, E. (1933). The laws governing the fineness of powdered coal. *Journal of the Institute of Fuel, 7*, 29–36.

Sanchidrián, J. A., Segarra, P., Ouchterlony, F., & López, L. M. (2009). On the accuracy of fragment size measurement by image analysis in combination with some distribution functions. *Rock Mechanics and Rock Engineering, 42*(1), 95–116. https://doi.org/10.1007/s00603-007-0161-8

Sazid, M., & Singh, T. N. (2013). Mechanism of air deck technique in rock blasting-a brief review. *Proceedings of the Indian Society for Rock Mechanics and Tunnelling Technology INDOROCK-2013*, New Delhi, India.

Sharma, P. D. (2010, June 26). *Application of air-deck technique in surface blasting*. Retrieved from https://miningandblasting.wordpress.com/2010/06/26/application-of-air-deck-technique-in-surface-blasting/

Siddiqui, F. I., Ali Shah, S. M., & Behan, M. Y. (2009). Measurement of size distribution of blasted rock using digital image processing. *Journal of King Abdulaziz University, 20*(2), 81–93. https://doi.org/10.4197/Eng.20-2.4

Spathis, A. T. (2004). A correction relating to the analysis of the original Kuz-Ram model. *Fragblast, International Journal for Blasting and Fragmentation, 8*(4), 201–205. https://doi.org/10.1080/13855140500041697

Stroud, R. (2010). *Life of mine plan Malundwe/ Kanga and Chimiwungo pits*. Perth, Australia: Optiro Pty Limited.

Split Engineering. (2001). Split-Desktop® [Computer software manual]. Tucson, AZ: Author.